MURAJ
Minnesota Undergraduate Research & Academic Journal
z.umn.edu/MURAJ

Lead Detoxification in *Priestia megaterium*

By Jamison Ward,[1] Beverly Flood,[1] Cara Santelli,[1] Michael Odlyzko,[2] Christof Zweifel,[1] Jake Bailey[1]

[1]Department of Earth and Environmental Sciences, University of Minnesota-Twin Cities, Minneapolis, Minnesota
[2]Characterization Facility, University of Minnesota-Twin Cities, Minneapolis, Minnesota

Abstract: Lead is a priority pollutant with an increasing environmental prevalence from human industrialization with deleterious consequences for both human and natural ecosystem health. In recent years, the application of lead-resistant microorganisms for bioremediation has received attention for its advantages over physiochemical remediation strategies. The bacterium *Priestia megaterium* has been previously observed to harbor lead resistance and accumulate lead intracellularly; however, our understanding of the mechanism for lead detoxification in this species remains incomplete. The present research employed a suite of analytical tools to investigate the mechanism of lead resistance in *P. megaterium* with lead sequestration in polyphosphate as the working hypothesis. Cells that were cultured in a lead-amended growth medium exhibited declining polyphosphate abundance with time, and spatial elemental analysis revealed that cells contained nanoparticles with an atomic composition similar to pyromorphite, suggesting that *P. megaterium* detoxifies lead by precipitating the metal with phosphate liberated from polyphosphate hydrolysis. Genomic analysis revealed that *P. megaterium* may export lead-phosphate precipitates from the cytoplasm via the Pit or Pst system. Furthermore, lead concentrations in the growth medium increased in the presence of the bacteria relative to abiotic controls, indicating that *P. megaterium* can solubilize abiotic lead precipitates in its environment. Collectively, these findings concur with previous observations of lead detoxification via lead-phosphate precipitation in other bacteria and have important implications for bioremediation strategies aiming to sequester lead within bacterial cells. Notably, the release of lead nanoparticles into aqueous solution may complicate efforts to remove lead from contaminated sites using polyphosphate-accumulating bacteria such as *P. megaterium*, necessitating the consideration of alternative lead removal techniques for environmental remediation efforts.

1. Introduction

Lead (Pb) is a priority pollutant with an increasing environmental prevalence from human industrialization due in large part to mining activities and commercial use in paints, pipes, pesticides, and gasoline.[1,2] Pb is a known human carcinogen and neurotoxin, and chronic exposure to Pb causes mental disorders, organ damage, and early death.[3] Furthermore, children from marginalized communities such as children of color or those from low-income families suffer increased risk of Pb poisoning relative to white children or those from wealthy families. This is because the former demographic is more likely to occupy older housing constructed with leaded paint or lead pipes and live near airports where exposure to emissions from small aircraft utilizing leaded gasoline is higher.[4,5] The widespread occurrence of Pb in the environment not only has deleterious consequences for human health but also negatively impacts the health of many natural ecosystems where Pb uptake by plants can lead to the biomagnification of Pb in food chains.[6] In regions of the world where humans consume organisms such as fish from contaminated waters, the concentration of Pb in higher trophic levels can exacerbate Pb poisoning in these populations.[6]

The toxicity of Pb mainly derives from its divalent oxidation state (Pb^{2+}), facilitating ionic exchange with other divalent cations such as magnesium (Mg^{2+}), calcium (Ca^{2+}), and iron (Fe^{2+}) which have similar ionic radii to Pb^{2+} and are essential for human neurological and cardiovascular function.[3,7] The chemical similarity of Pb to these metals also permits non-specific uptake by microorganisms; in particular, Pb has been observed to accumulate within polyphosphate granules in bacteria growing in Pb-rich environments.[8–11] Polyphosphate (polyP) granules are nanometer-scale intracellular inclusions composed of phosphate polymers that many microorganisms synthesize for cellular phosphorus and energy storage and which contain metal cations such as Ca^{2+} and Mg^{2+} to neutralize the negatively charged phosphate monomers.[12] Consequently, polyP granules have the capacity to sequester chemically mobile Pb ions within a bacterial cell, reducing the bioavailability of the metal in both the cytoplasmic and extracellular environment.[13] Despite this potential, little research has been conducted to evaluate Pb accumulation in microbial polyP granules as a bioremediation technique.

This study investigated the Pb resistance mechanism of *Priestia megaterium* (formerly *Bacillus megaterium*),[14] a Gram-positive, polyP-accumulating bacterium native to soil environments and known to harbor Pb resistance and precipitate Pb intracellularly. The second objective of this study was to evaluate the potential of *P. megaterium* to remove Pb from an aqueous solution as a putative bioremediation technique. From our analyses, we suggest that *P. megaterium* may degrade its polyP to precipitate Pb as Pb-phosphate nanoparticles and subsequently efflux them from the cell. Furthermore, we suggest that *P. megaterium* can solubilize abiotic Pb precipitates to obtain sulfate, increasing the concentration of soluble Pb in the immediate environment of the organism.

2. Materials and Methods

2.1. Culture Conditions and Growth Curve

The model organism *Bacillus megaterium* ATCC 6459 (hereafter "*Priestia megaterium*")

was obtained from the United States Department of Agriculture Agricultural Research Service Culture Collection (Northern Regional Research Laboratory) and was originally isolated from Virginia, USA soil. Cells were cultured in a shaking incubator at 28°C and 150 rpm in a minimal medium[15] consisting of the following reagent-grade components (g/L) buffered at pH 6.0: glucose monohydrate (2.20), 2-(*N*-morpholino)-ethanesulfonic acid hydrate (MES, 1.95), KCl (0.020), $MgSO_4 \cdot 7\ H_2O$ (0.240), $CaSO_4 \cdot 2\ H_2O$ (0.044), NH_4Cl (0.050), $NaNO_3$ (0.170), NaH_2PO_4 (0.00845), $(NH_4)_2Fe(SO_4)_2 \cdot 6\ H_2O$ (0.00564), and 1 mL/L of SL7 trace element solution[16] consisting of (mg/L) $ZnCl_2$ (70), $MnCl_2 \cdot 4\ H_2O$ (100), H_3BO_3 (60), $CoCl_2 \cdot 6\ H_2O$ (200); $CuCl_2 \cdot 2\ H_2O$ (20), $NiCl_2 \cdot 6\ H_2O$ (20), $NaMoO_4 \cdot 2\ H_2O$ (40). All reagents were prepared in ultrapure Type 1 water with 18.2 MΩ·cm resistivity at 25°C (hereafter "Type 1 water") from a Milli-Q water purification system (MilliporeSigma (Merck KGaA), Darmstadt, Germany) and filtered sterilized using 0.22 µm pore size polyethersulfone (PES) membrane filters. The growth medium was designed to maximize the concentration of soluble Pb ions and therefore excluded undefined components such as yeast extract or tryptone, which significantly decrease heavy metal ion bioavailability via chelation.[17,18] Kickstarter cultures in 18 mm glass test tubes were grown to an optical density (OD) measured at 600 nm of ~0.6 after which a single kickstarter culture was used to inoculate three replicate trials in 25 mm glass test tubes using a 1:100 (v/v) inoculum. Three abiotic control trials were also prepared and incubated under the same conditions.

After culturing *P. megaterium* to stationary phase in the Pb-free growth medium to promote substantial polyP accumulation, each culture was transferred to a medium of the same composition but which was amended with a final concentration of 100 µM Pb and excluded NaH_2PO_4 to circumvent Pb-phosphate precipitation.[17] The Pb-amended medium contained $Pb(NO_3)_2$ (0.033 g/L) and $NaNO_3$ (0.153 g/L) to maintain equimolar concentrations of NO_3^- between the two types of media. Additionally, the Pb-amended medium was buffered at pH 5.6 to prevent Pb-carbonate precipitation with dissolved CO_2 from the ambient laboratory air. Stationary phase cultures in the Pb-free medium were poured into sterile 15 mL conical tubes and centrifuged at 7,197 RCF for 5 minutes to obtain cell pellets. After discarding the supernatants, cell pellets were washed twice by centrifuging at 7,197 RCF for 5 minutes in a solution of 10 mM MES and 12 mM NaCl at pH 6.0 to remove residual phosphorus from the cells and then resuspended in 10 mL of Pb-amended minimal media. Finally, each biological sample was added to 25 mm glass test tubes containing 10 mL of Pb-amended media to give a final volume of 20 mL per trial. Three abiotic controls containing 20 mL of Pb-amended media were also prepared in 25 mm test tubes. All six trials were then cultured in a shaking incubator at 28°C and 150 rpm.

At 12-hour intervals in both Pb-free and Pb-amended incubations, 1 mL aliquots from each trial were transferred into 1.5 mL microcentrifuge tubes and centrifuged at 10,000 RCF for 5 minutes to obtain cell pellets. The supernatants were aspirated and stored at -20°C in separate 1.5 mL microcentrifuge tubes until further analysis. Cell pellets were resuspended in 250 µL of fixative solution consisting of 2% (w/v) paraformaldehyde and 12 mM NaCl for 12 hours

at 4°C. After this, cell samples were centrifuged at 10,000 RCF for 5 minutes to remove the fixative agent, resuspended in 500 µL preservative solution consisting of 50% (v/v) ethanol, 10 mM MES, and 12 mM NaCl at pH 6.0, and then centrifuged at 10,000 RCF for 5 minutes. After discarding the supernatant, the washing procedure was repeated a second time before the cells were resuspended in 500 µL of the preservative solution and stored at -20°C until further analysis. At each sampling point, additional 1 mL culture aliquots from each trial were transferred to semi-micro UV cuvettes to measure the culture OD using a Spectronic 20D+ spectrophotometer (Thermo Fisher Scientific, Waltham, Massachusetts, USA). Aliquots from one of the abiotic control trials served as OD blanks to zero the spectrophotometer. When necessary, culture aliquots were appropriately diluted with uninoculated growth medium from a stock kept at 28°C in the incubator to reduce the measured OD below 0.4 to ensure a linear response from the spectrophotometer.[19,20]

A subset of the supernatant samples obtained from the Pb-amended medium was filter sterilized to remove any large precipitates before acidifying the samples for Pb quantification. For each aliquot, 400 µL of supernatant was aspirated into a 1 mL sterile syringe, passed through a 0.22 µm pore size PES membrane filter into a new 1.5 mL microcentrifuge tube, and stored at -20°C until further analysis.

2.2. Mass Spectrometry

Pb concentrations in the growth medium were quantified using inductively coupled plasma mass spectrometry (ICP-MS). Supernatant samples from the Pb-amended cultures were analyzed using an iCAP TQ triple quadrupole inductively coupled plasma mass spectrometer (Thermo Fisher Scientific, Waltham, Massachusetts, USA) at the University of Minnesota Department of Earth and Environmental Sciences Analytical Geochemistry Laboratory. Nitric acid matrix-matched Pb standards were prepared from a NIST-traceable heavy metals plasma standard (Alfa Aesar, Ward Hill, Massachusetts, USA) in 2% HNO_3 diluted from 69% (w/w) trace element grade HNO_3 (Sigma-Aldrich, Burlington, Massachusetts, USA) using Type 1 water. Pb concentrations were quantified using a 10 ppb ^{193}Ir internal standard. Supernatant samples were initially digested by diluting 5x in 20% HNO_3 and then diluted an additional 100x in 2% HNO_3 to give a final dilution of 500x before analysis.

2.3. Epifluorescence Microscopy

Epifluorescence microscopy was employed to track cellular polyP abundance before and after transfer to the Pb medium. Cell samples were co-stained with two fluorophores to visualize polyP granules: 4′,6-diamidino-2-phenylindole (DAPI) and tetracycline hydrochloride (TC). DAPI is a DNA-binding fluorescent stain with a DNA-DAPI complex emission spectrum peak at 461 nm when excited by ultraviolet light at 372 nm. DAPI can also form a complex with polyP, which causes the fluorescence emission peak to intensify and shift to 526 nm, producing a green color.[21] TC is an antibiotic with fluorescent properties and a chelator of divalent cations. When excited by ultraviolet light at 390-425 nm, TC has an emission spectrum from 510-560 nm, producing a yellow-green color.[22] Since polyP contains divalent cations that neutralize the negative

charges of the phosphate monomers,[12] TC binds to polyP granules at higher concentrations than background levels within the cell. Thus, the combination of DAPI and TC stains effectively labels polyP granules for epifluorescence microscopy examination. For each sample, 100 µL of fixed cell suspension was transferred to a microcentrifuge tube and centrifuged at 10,000 RCF for 5 minutes to obtain a cell pellet. After discarding the supernatant, cells were resuspended in 100 µL of freshly prepared 0.2 mM TC solution.[23] Cells were stained for 10 minutes in the dark after which 400 µL of Type 1 water was added to dilute the cell suspension back to the original sample concentration. Next, 10 µL of TC-stained cell suspension was pipetted onto a glass microscope slide and allowed to air dry in the dark. Once dry, the cell deposit was stained for 30 minutes in the dark with 10 µL of 5 µg/mL DAPI solution pipetted directly onto the microscope slide. Slides were subsequently rinsed with Type 1 water to remove excess DAPI stain and blotted dry with a Kimwipe. Finally, 5 µL of CitiFluor antifadent solution (Electron Microscopy Sciences, Hatfield, Pennsylvania, USA) was pipetted onto the cell deposit before applying a coverslip to the microscope slide to protect the specimen from photobleaching.

DAPI- and TC-stained cell samples were examined using an Olympus BX61 epifluorescence microscope (Olympus Corporation, Shinjuku, Tokyo, Japan) connected to an Olympus BX-UCB microscope control unit and a Lumen 200 200-watt metal halide arc lamp (Prior Scientific, Cambridge, UK). Cells were imaged in two different viewing modes: fluorescent excitation and phase contrast. In fluorescent mode, two different optical filter cubes were used to provide different viewing conditions of stained samples (Semrock, Inc., Rochester, New York, USA). The first was a DAPI long pass filter cube with a 350/50x nm excitation filter and a 425 nm long pass emission filter. The second was a custom polyP filter with a 420/20x nm excitation filter and a 540/40m nm emission filter. Image capture and annotation were performed using Olympus cellSens software. Aside from imprinting magnification and scale information and adjusting image brightness, no visual modifications were applied to fluorescence microscopy images.

2.4. Electron Microscopy

Sanning-transmission electron microscopy coupled with energy-dispersive x-ray spectroscopy (STEM-EDS) was used to examine fine-scale cellular morphology and elemental distribution within biological specimens. To prepare samples for STEM-EDS analysis, 100 µL of fixed, unstained cells were centrifuged at 10,000 RCF for 5 minutes to obtain a cell pellet. Next, cells were washed twice by centrifuging the samples at 10,000 RCF for 5 minutes in Type 1 water to remove surface-bound salts from the preservative solution. Whole cell samples were then drop cast onto 200-mesh Cu TEM grids with Lacey Formvar/carbon support film (Ted Pella, Inc., Redding, California, USA) and allowed to dry in open air overnight.

Electron microscopy analysis was performed at the University of Minnesota Characterization Facility using a Talos F200X G2 transmission electron microscope (Thermo Fisher Scientific, Waltham, Massachusetts, USA) coupled to a Thermo Fisher X-FEG Schottky FEG electron source at 200 keV beam energy and equipped with high-angle annular dark field Fischione Model 3000 HAADF and low-angle

annular dark field Thermo Fisher DF4 STEM detectors and a Thermo Fisher Super-X G2 X-ray detector. When acquiring elemental maps, the microscope was set to a 7.5 mrad convergence semi-angle and 2.0 nA beam current, providing a best resolution of ~1 nm; in this setting, the HAADF detector collected 46-200 mrad and the DF4 detector collected 18-44 mrad. Bright regions in HAADF images signify features with high material thickness along the beam axis and high atomic mass within the feature. Image and EDS map acquisition as well as data post processing were performed using Thermo Fisher Velox software. Standardless, semi-quantitative elemental quantification was performed using L lines for Pb and K lines for all other elements. Sulfur quantification was not possible due to peak overlap between Pb M lines and sulfur K lines.

3. Results

3.1. Cell Growth and Morphology

P. megaterium cultures reached stationary growth phase after ~36 hours of incubation in the Pb-free medium and were transferred to the Pb-amended medium after 60 hours of incubation (Fig. 1a). Epifluorescence microscopy imaging revealed that *P. megaterium* cells appeared as ovate rods, often in pairs or chains, at early sampling points in the Pb-free medium, but cell morphology became progressively stubby and shriveled beyond 12 hours of incubation (Fig. 2). Additionally, cells collected after 12 hours in the Pb-free medium exhibited a color dichotomy when viewed using the DAPI long pass filter cube wherein increasingly more cells appeared blue while fewer cells appeared green as time progressed (Fig. 2b-d). At the time of transfer to the Pb medium, a large proportion of cells contained bright greenish-yellow bodies at their poles indicating the presence of polyP granules and thus permitting the investigation of Pb-polyP dynamics (Fig. 2d). Notably, when using the DAPI long pass filter cube to examine the cells, polyP granules appeared exclusively in fluorescent blue cells while fluorescent green cells did not possess these features (Fig. 2b-d).

Culture density in the Pb-amended medium decayed with time, decreasing to less than half of the initial OD after 96 hours of incubation (Fig. 1b). Furthermore, cell samples from Pb-amended trials exhibited decreasing polyP abundance with time, with few discernable polyP granules present in cells after 96 hours (Fig. 3a-d). Coincident with the decline in cellular polyP abundance was the appearance of precipitate-like entities after 12 hours in the Pb-amended medium. These entities were opaque when viewed with fluorescent excitation but transparent when viewed using phase contrast light (Fig. 3). Furthermore, when viewed using the DAPI long pass filter cube, these features appeared exclusively in fluorescent green cells. Samples acquired from the Pb-amended incubations at later time points contained a greater abundance of cells harboring these precipitate-like features (Fig. 3b-d).

3.2. Cellular Elemental Analysis

Electron microscopy imaging revealed that a significant proportion of cells collected at 12 hours or later from the Pb-amended medium possessed putative intracellular or surface-associated nanoparticles exhibiting different distribution patterns (Fig. 4a-f). In some cells, the nanoparticles were zoned toward the cell poles (Fig. 4c) whereas in others, the nanoparticles

were omnipresent on or within the cell (Fig. 4e). Spatial elemental analyses revealed that these nanoparticles were strongly enriched in Pb and slightly enriched in P and Cl relative to the near-uniform distributions of C, N, and O throughout the cell (Fig. 5). Semi-quantitative EDS analyses of seven selected Pb-rich features indicated that the average normalized atomic percentages of Pb, P, and Cl were 49.6 ± 2.5, 37.1 ± 2.7, and 13.4 ± 1.1, respectively, where the error represents the 95% confidence interval. These results are only semi-quantitative due to systematic EDS experimental errors including uncertainties of absorption cross sections, X-ray absorption by cellular features, and position-dependent X-ray absorption. Regardless, the normalized atomic percentages of Pb, P, and Cl in all seven Pb-rich features cluster closely together in Pb-P-Cl space (Fig. 6). Fig. 7 provides a representative EDS spectrum and atomic percentage values for one of these Pb-rich features.

3.3. Pb Concentrations in the Culture Medium

Abiotic control trials exhibited a soluble Pb concentration of approximately 50 μM (i.e., half the formulated concentration of 100 μM Pb in the growth medium) throughout the experiment when unfiltered supernatants were analyzed (Fig. 8a) and slightly less than 30 μM Pb when filtered supernatants were analyzed (Fig. 8b). In both cases, abiotic supernatant Pb concentrations were stable throughout the 144-hour incubation. In contrast, biotic trials exhibited increasing Pb concentration with time, rising to above 90 μM (i.e., 90% of the formulated Pb concentration) after 144 hours regardless of whether the supernatants were filtered (Fig. 8a-b). In both cases, the supernatant Pb concentration sharply increased after the first 12 hours of incubation. For the biotic trials, the Pb increase in the first 12 hours accounted for 76 ± 23% of the total Pb increase over 144 hours when supernatants were unfiltered and accounted for 69 ± 3.1% of the total Pb increase when supernatants were filtered.

4. Discussion

The application of Pb-resistant microorganisms for bioremediation has received considerable attention in recent decades for its advantages over physiochemical remediation strategies, which are less cost-effective, more difficult to implement, and often create secondary waste when compared to biological remediation methods.[24,25] Current Pb bioremediation strategies mainly exploit microbial extracellular Pb immobilization mechanisms such as biosorption to the cell surface or extracellular matrix, extracellular precipitation, or binding by siderophores.[24–27] However, intracellular Pb precipitation has also been observed to occur in microorganisms via chelation by small, cysteine-rich metallothionein proteins, which reduces the bioavailability of toxic metals within a cell.[24–26] One study proposed that this mechanism was responsible for intracellular Pb precipitation in a Pb-resistant *P. megaterium* strain; however, the results of this study provided no conclusive evidence to support this claim.[28] Another known mechanism of intracellular Pb detoxification occurs via precipitation with phosphate anions followed by export from the cell.[13,24,25] Here, polyP plays an important role in serving as a source of phosphate anions to bind and chemically immobilize toxic heavy metals prior to efflux.[13,29,30] Alternatively, other studies have reported that polyP can directly sequester Pb ions

as constitutive cations.[8–11] We report evidence that *P. megaterium* hydrolyzes polyP to detoxify intracellular Pb cations as insoluble Pb-phosphate precipitates with a chemical composition similar to pyromorphite.

4.1. Cell Physiology and PolyP Dynamics

The manifestation of two distinct *P. megaterium* cell physiologies was a striking observation in this experiment. When cells in late exponential to stationary growth phase were observed using the DAPI long pass filter cube, the bacteria fluoresced in two different colors, and the presence of polyP granules correlated with cell color. While a significant proportion of fluorescent blue cells harbored polyP granules, fluorescent green cells never possessed distinct polyP granules (Fig. 2b-d). Knowing that the DNA-DAPI complex fluoresces blue while the polyP-DAPI complex fluoresces green when excited by UV light,[21,22] we interpret these observations to reflect the nature of polyP organization in the cells; namely, blue cells form discrete polyP granules in response to P limitation in the growth medium while green cells instead contain diffuse intracellular polyP. The shriveled and stubby morphology of cells collected at time points after 12 hours in the Pb-free medium (Fig. 2b-d) and at all time points in the Pb-amended medium (Figs. 3a-d, 4b-f) further signifies that the bacteria were under stress conditions, most likely nutrient starvation in the form of P limitation.

When the cells were transferred to the P-free, Pb-amended medium, fluorescent blue cells exhibited a trend of declining polyP granule abundance with time (Fig. 3a-d), indicating that these cells were degrading their polyP granules in response to P starvation and potentially to detoxify Pb taken up non-specifically from the growth medium via Pb-phosphate precipitation.[12,13] Several previous studies have documented declining polyP abundance in various bacteria and microeukaryotes exposed to a variety of heavy metals, including Pb, suggesting that polyP hydrolysis plays an active role in heavy metal detoxification.[31–33] However, one experiment involving *Diatoma elongatum* revealed no change in the abundance of polyP bodies upon exposure to Pb; rather, the polyP bodies within the diatom were observed to bind Pb, thereby immobilizing the metal within the intracellular environment.[8] These contrasting observations indicate that the role of polyP in cellular Pb detoxification varies among different organisms. In particular, one study suggests that eukaryotes preferentially employ intracellular sequestration mechanisms whereas prokaryotes tend to utilize active pumping mechanisms to remove toxic metals from the cell cytoplasm.[34]

4.2. Cellular Pb Precipitation

Evidence for cellular precipitation of Pb manifests in both fluorescence and electron microscopy studies of *P. megaterium* cell samples. After 12 hours in the Pb-amended medium, precipitate-like features developed exclusively in fluorescent green cells that appeared opaque when viewed using fluorescent light and transparent when viewed using phase contrast light (Fig. 3b-d). Furthermore, these features became increasingly abundant with time in the Pb-amended medium (Fig. 3a-d). We interpret these features as Pb precipitates as they were absent in cells harvested from the Pb-free medium and only formed once the bacteria were transferred to the Pb-amended medium. However, the formation of these features is not

directly coupled to the observation of declining polyP granule abundance in the Pb-amended medium as the Pb precipitates only occurred in fluorescent green cells while polyP granules were only present in fluorescent blue cells.

Electron microscopy analyses of cell samples revealed the presence of nanoparticles associated with a substantial proportion of bacteria harvested from the Pb-amended medium (Fig. 4). These nanoparticles were strongly enriched in Pb and moderately enriched in P and Cl relative to background cellular abundances (Fig. 5). Based on this first-order elemental analysis, these nanoparticles could be pyromorphite [$Pb_5(PO_4)_3Cl$], a Pb-chlorophosphate mineral from the apatite group with normalized atomic percentages of Pb, P, and Cl of 55.6, 33.3, and 11.1, respectively.[35] Importantly, as the Pb-amended medium was formulated without P, these Pb-phosphate nanoparticles must have been produced via biological processes, indicating that the cells expended a portion of their P supply to form the Pb-phosphate nanoparticles. Several prior studies have demonstrated biologically induced pyromorphite precipitation by various bacteria exposed to Pb,[36–38] indicating that this Pb detoxification mechanism exists broadly among prokaryotes. Thus, *P. megaterium* may also detoxify intracellular Pb by immobilizing the metal via pyromorphite precipitation.

Previous studies of intracellular heavy metal detoxification in microorganisms suggest a mechanism wherein the exopolyphosphatase (PPX) enzyme hydrolyzes the terminal phosphate residue of polyP in response to rising intracellular metal cation concentrations to precipitate the toxic metal as a metal phosphate ($MeHPO_4$).[30,33,39] Following this, the cell effluxes $MeHPO_4$ via a phosphate transporter such as the constitutive phosphate inorganic transport (Pit) system or the inducible phosphate-specific transport (Pst) system described in *Escherichia coli*.[30,40] The Pit system harnesses the membrane proton motive force to transport inorganic phosphate (P_i) via P_i-H^+ symport while the Pst system relies upon both the membrane potential and ATP hydrolysis to transport P_i across the cell membrane.[40] Furthermore, the Pit system has been shown to function as a $MeHPO_4$ transporter in *E. coli*, enabling the coupled import and export of P_i and divalent metal cations in the bacterium.[39]

A separate transport system involving P-type ATPases (e.g., ZntA, CadA, PbrA) has also been found to confer heavy metal resistance in both Gram-positive and Gram-negative bacteria.[34,41,42] The mechanism involves the efflux of divalent metal cations such as Cd^{2+} and Zn^{2+} but has also been shown to non-specifically efflux Pb^{2+} cations in *E. coli* (ZntA), *Staphylococcus aureus* (CadA), and *Cupriavidus metallidurans* (PbrA).[34,41,42] In *C. metallidurans*, Pb^{2+} ions extruded into the periplasm precipitate with P_i ions released from the carrier lipid undecaprenyl pyrophosphate by PbrB, an undecaprenyl pyrophosphate phosphatase, preventing Pb from reentering into the cytoplasm.[34]

To assess potential mechanisms that could facilitate Pb-phosphate or Pb^{2+} cation efflux from *P. megaterium*, we queried for gene product names containing the terms "phosphate" and "transporter" in all 102 permanent draft and finished *Priestia megaterium* genomes in the Department of Energy's Joint Genome Institute Integrated Microbial Genomes collection.[43] Of these 102 genomes, 99 contained at least one gene encoding a Pit family inorganic phosphate

transporter, and 97 contained at least one gene encoding a component of the Pst system. We also queried for gene product names containing the term "P-Type ATPase" and found that 66 of the 102 *Priestia megaterium* genomes contained at least one gene encoding a cation-transporting P-Type ATPase. Based on these findings, it is likely that the *P. megaterium* strain investigated in this study could extrude Pb from the cytoplasm via $MeHPO_4$ efflux mediated by the Pit or Pst system; additionally, *P. megaterium* may have the capability to directly export Pb^{2+} cations using a P-Type ATPase. In the latter case, the bacterium would also need to expel P_i to chemically immobilize Pb^{2+} as a Pb-phosphate precipitate. *P. megaterium* could accomplish this by passively exporting P_i hydrolyzed from polyP by PPX using the Pit system. Once the extruded Pb^{2+} ion precipitates with P_i in the extracellular environment, the Pb would be unable to reenter the cell as most Pb-phosphate minerals are highly insoluble at all environmentally relevant pH values (Fig. 9).

4.3. Biotic Effect on Pb Concentration

It is evident from Fig. 8 that abiotic Pb precipitation occurred during the experiment despite no visible precipitates in the abiotic control media as the measured soluble Pb concentration in abiotic trials was ~30 µM and ~50 µM (i.e., less than the formulated concentration of 100 µM) when supernatant samples were analyzed with and without filtration, respectively. This implies that a portion of abiotic Pb precipitates were separated from the supernatant during centrifugation and thus the Pb was not recovered by digestion in HNO_3 for ICP-MS quantification. As the membrane filters used had a pore size of 0.22 µm, the Pb concentration of ~30 µM represents the concentration of soluble Pb plus any Pb precipitates in the supernatant smaller than 0.22 µm while the Pb concentration of ~50 µM reflects the concentration of soluble Pb plus Pb precipitates of any size remaining in the supernatant after centrifugation. Since these two values differ, the filter sterilization process removed some suspended Pb particles greater than 0.22 µm in size from the supernatant samples. Based on thermodynamic modeling in The Geochemist's Workbench (GWB) geochemical modelling software,[44] the Pb-amended growth medium used in this experiment was slightly oversaturated with two Pb minerals, anglesite (Q/K = 3.295) and lanarkite (Q/K = 1.367), both of which are Pb-sulfate minerals. When these minerals were allowed to precipitate from the modeled growth medium, the calculated Pb^{2+} concentration was 30.5 µM, which agrees with the ~30 µM Pb concentration measured in filter sterilized supernatants. Therefore, we conclude that the Pb-amended growth medium contained a final soluble Pb concentration of ~30 µM due to the abiotic precipitation of Pb-sulfate minerals from the oversaturated solution containing Pb^{2+} from $Pb(NO_3)_2$ and SO_4^{2-} from $MgSO_4 \cdot 7\ H_2O$, $CaSO_4 \cdot 2\ H_2O$, and $(NH_4)_2Fe(SO_4)_2 \cdot 6\ H_2O$.

The biotic supernatant samples had an initial Pb concentration overlapping within error of the initial Pb concentration in the abiotic supernatants regardless of whether the supernatants were filtered. However, in both cases, the supernatant Pb concentration increased to over 90 µM in biotic trials (Fig. 8). Therefore, the increase in Pb concentration due to the presence of the bacteria is mostly in the form of soluble Pb and/or Pb precipitates smaller

than 0.22 μm. As shown in STEM images, the cell-associated Pb nanoparticles were mostly less than 220 nm in size (Fig. 4), so these biological precipitates could have passed through the membrane filter when supernatants were filtered, contributing to a higher measured Pb concentration when samples were acidified with HNO_3 for ICP-MS analysis. Furthermore, the fact that the Pb concentration in the biotic trials increased to nearly 100 μM indicates that the bacteria solubilized most of the abiotically precipitated Pb-sulfate minerals that were removed from the abiotic supernatants via centrifugation and filter sterilization. There are several potential mechanisms by which *P. megaterium* could have solubilized the Pb-sulfate precipitates. Firstly, acidification of the Pb-amended, P-free growth medium below pH 5.5 would have resulted in lanarkite undersaturation; however, continued acidification would not result in anglesite undersaturation until pH < 2, which is unlikely to have occurred given that the growth medium was buffered at pH 5.6 with 10 mM MES. Alternatively, continued uptake of dissolved SO_4^{2-} ions by *P. megaterium* would have eventually caused undersaturation of both lanarkite and anglesite once the SO_4^{2-} concentration dropped below 0.75 mM and 0.30 mM, respectively, thereby releasing Pb^{2+} ions into solution. The bacterium could then export any cytoplasmic Pb taken up non-specifically from the growth medium as Pb-phosphates via the Pit or Pst system as discussed in section 4.2. These Pb-phosphate precipitates would remain insoluble even if *P. megaterium* significantly acidified the growth medium (Fig. 9), effectively preventing Pb reentry into the cell.

5. Conclusions

The soil bacterium *Priestia megaterium* exhibits dynamic intracellular behavior when stationary-phase, polyP-bearing cells are exposed to a Pb-containing growth medium. Over time, cells degrade their polyP granules and form Pb nanoparticles with a composition similar to pyromorphite. Future STEM-tomography studies could elucidate whether the observed Pb nanoparticles reside inside or outside of cells, or perhaps both, and therefore determine whether *P. megaterium* employs an intra- or extracellular Pb detoxification mechanism. Additionally, *P. megaterium* can putatively solubilize abiotically precipitated Pb-sulfate minerals by taking up SO_4^{2-} from the growth medium, which increases the soluble Pb concentration in the immediate environment. Both the formation of Pb nanoparticles and Pb-sulfate solubilization by *P. megaterium* have important implications for Pb bioremediation techniques. Namely, the release of Pb nanoparticles into solution may complicate efforts to remove Pb from contaminated sites via biological sequestration using polyP-accumulating bacteria such as *P. megaterium*. Furthermore, the solubilization of preexisting abiotic Pb precipitates via biological nutrient uptake underscores the importance of considering alternative Pb removal strategies for environmental restoration efforts. While overall the metabolic activity of *P. megaterium* increases soluble Pb concentrations in aqueous solutions by solubilizing Pb-sulfate minerals and precipitating Pb nanoparticles to detoxify intracellular Pb, genetic engineering to inhibit the putative Pb efflux mechanisms of the bacterium may improve the suitability of *P. megaterium* for Pb bioremediation applications.

Acknowledgments

Funding for this research was provided by the University of Minnesota Office of Undergraduate Research and the Minnesota Undergraduate Research and Academic Journal. Additionally, parts of this work were conducted at the University of Minnesota Characterization Facility, which receives partial financial support from the NSF through the MRSEC (Award Number DMR-2011401) and the NNCI (Award Number ECCS-2025124) programs. The ternary diagram in Fig. 6 was created using open source Python code.[45]

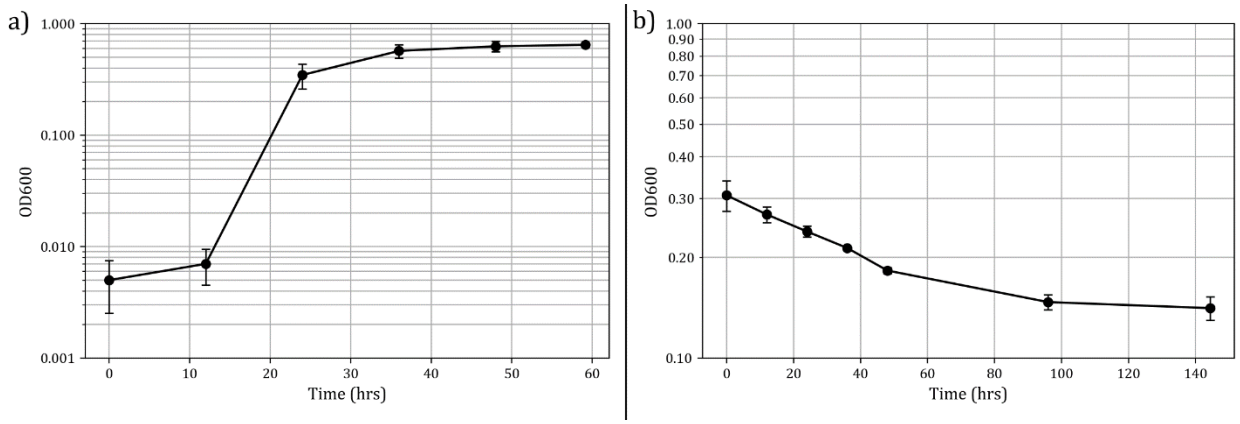

Figure 1a-b. Growth curves of *P. megaterium* culture optical density in the a) Pb-free medium and b) medium amended with 0.10 mM Pb. Note the differing y axis scales. All error bars represent 95% confidence intervals from three replicate trials. Error bars not visible are smaller than the data point marker.

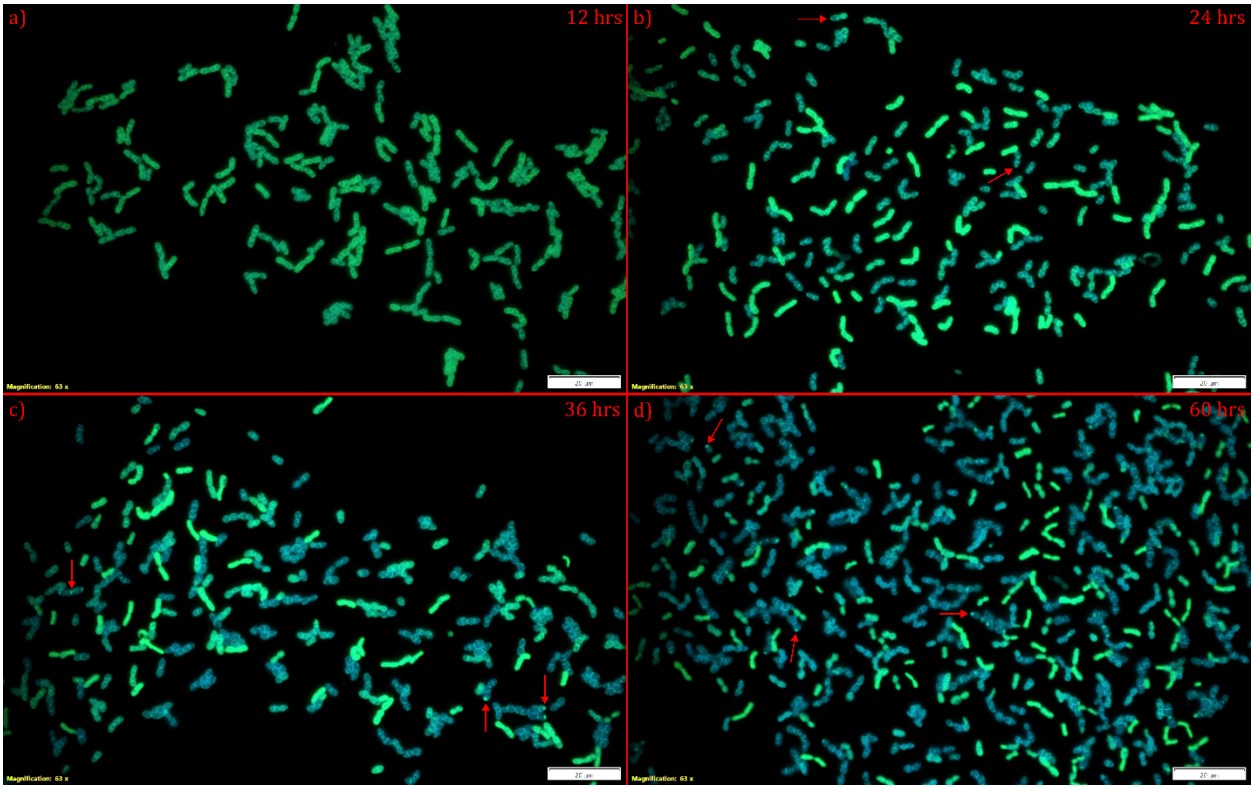

Figure 2a-d. Fluorescence microscopy images of DAPI and TC-stained cells harvested from the Pb-free medium at a) 12 hours, b) 24 hours, c) 36 hours, and d) 60 hours viewed using the DAPI long pass filter cube. The red arrows indicate polyP granules that manifested after 24 hours and occurred more frequently in cells at later time points.

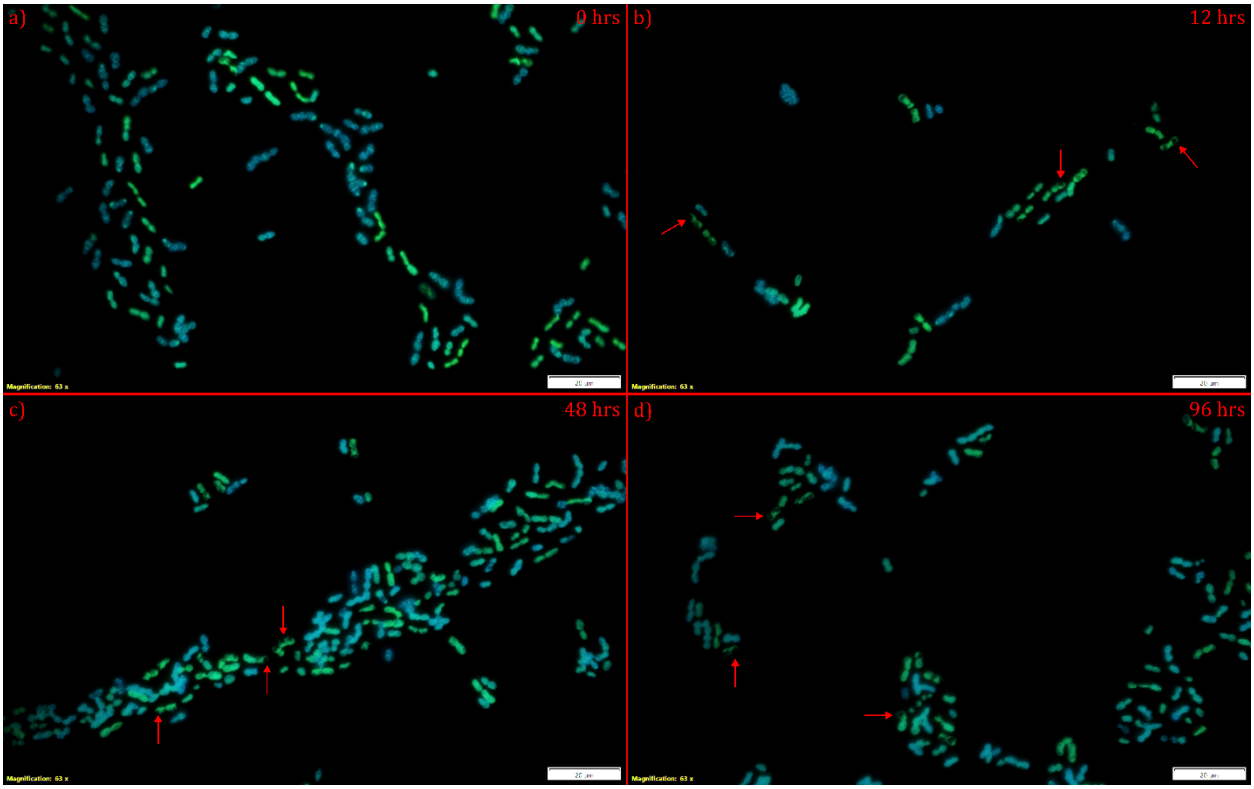

Figure 3a-d. Fluorescence microscopy images of DAPI and TC-stained cells harvested from the Pb-amended medium at a) 0 hours, b) 12 hours, c) 48 hours, and d) 96 hours viewed using the DAPI long pass filter cube. The red arrows indicate opaque precipitate-like features that manifested after 12 hours and occurred more frequently in cells at later time points. Also note the decreasing abundance of bright polyP granules with time.

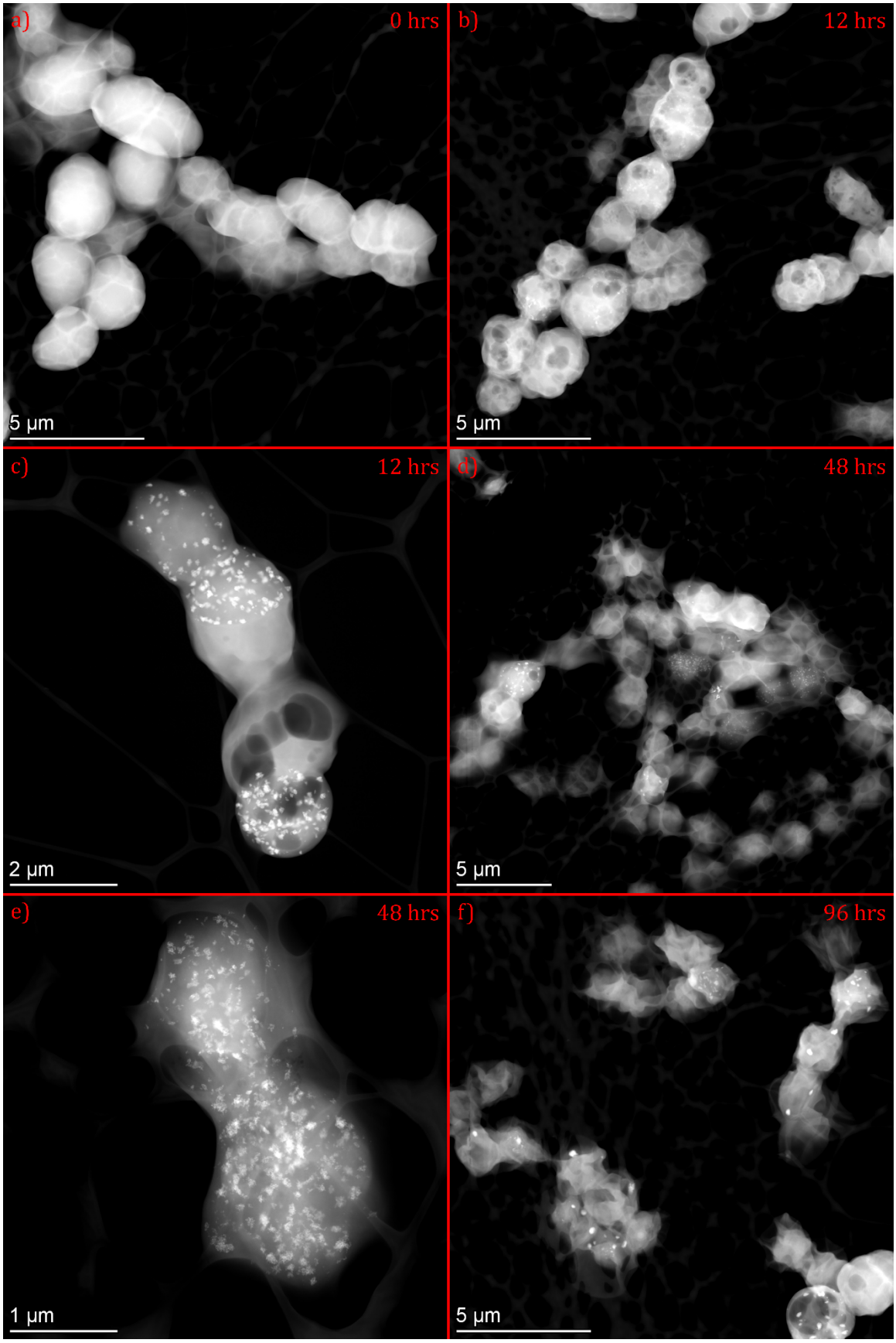
a)
0 hrs
5 µm
b)
12 hrs
5 µm
c)
12 hrs
2 µm
d)
48 hrs
5 µm
e)
48 hrs
1 µm
f)
96 hrs
5 µm

Figure 4a-f (previous page). HAADF-STEM images of cell samples collected at various time points from the Pb-amended growth medium. Note that the bright nanoparticles are nearly absent at time zero but become more prominent at later time points. The large, dark voids in cells represent damage from prolonged exposure to the 200 keV electron beam.

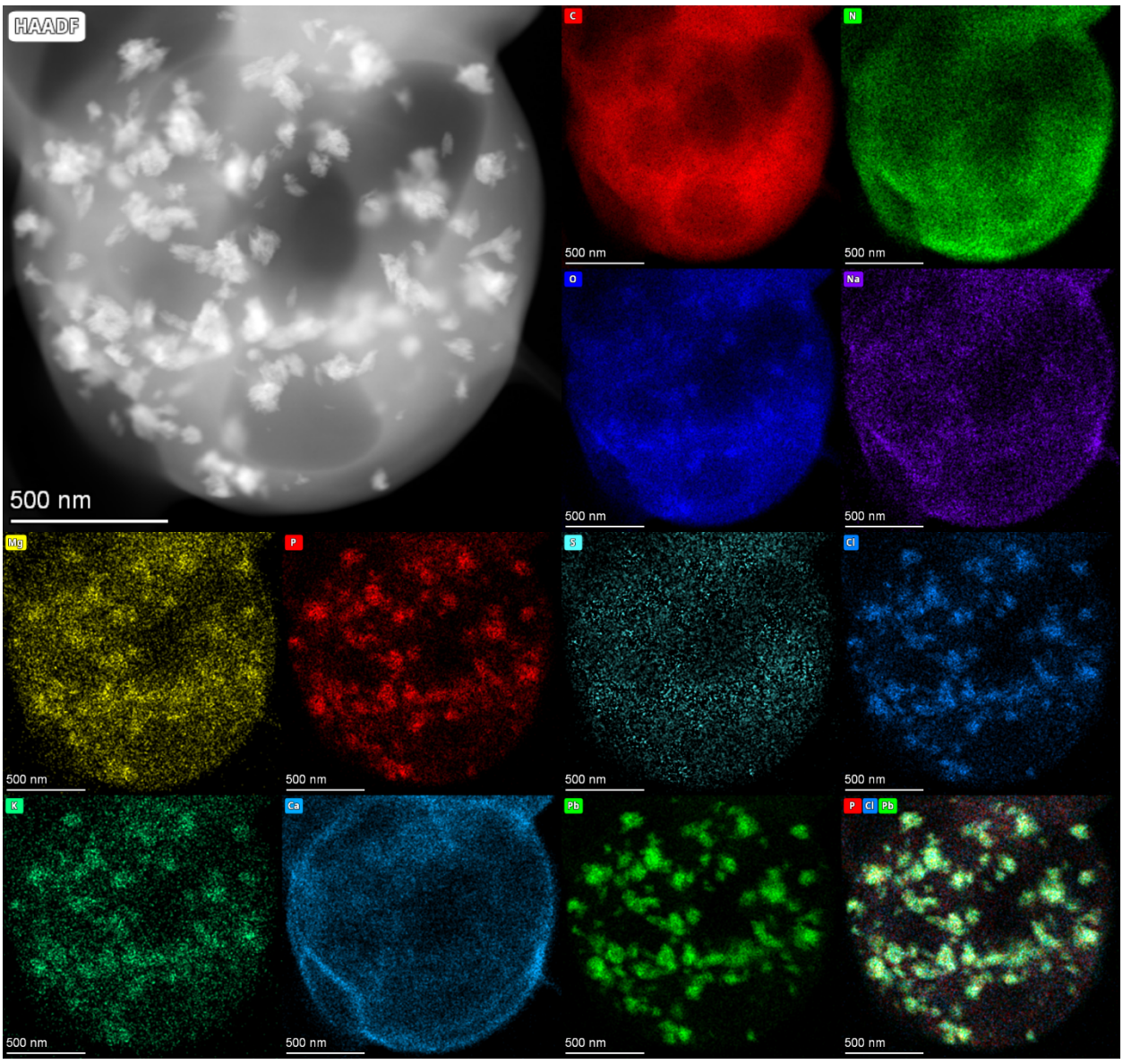

Figure 5. Elemental maps of nanoparticles at the bottom end of the cell in Fig. 4c collected after 12 hours in the Pb-amended medium. The white regions in the bottom right pane represent areas where Pb (green), P (red), and Cl (blue) are spatially coincident. The large, dark voids in cells represent damage from prolonged exposure to the 200 keV electron beam of the STEM.

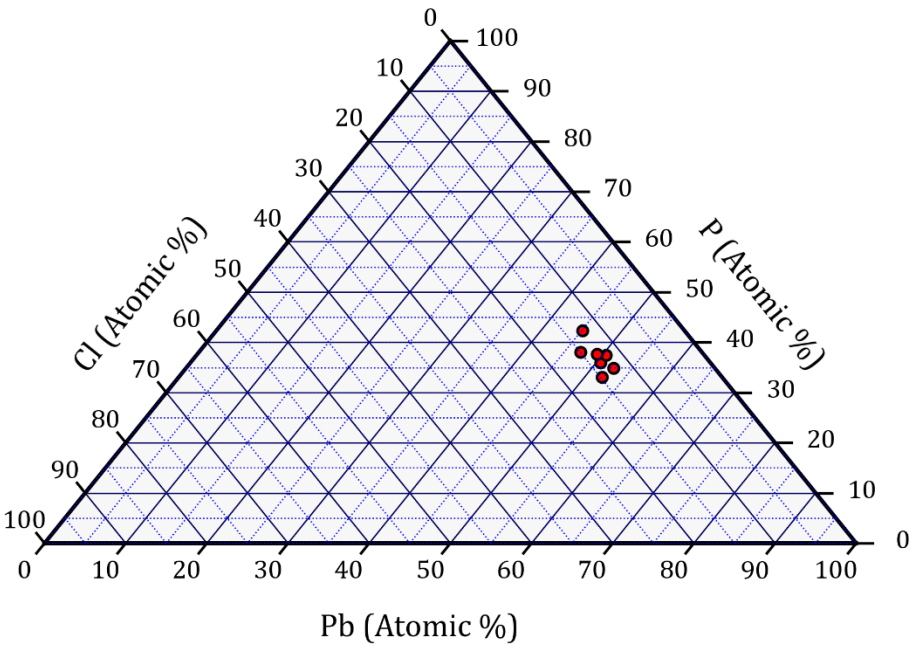

Figure 6. Ternary diagram depicting the normalized atomic percentages of Pb, P, and Cl in seven selected Pb-rich features in cells harvested from the Pb-amended growth medium at various time points. Note that the atomic compositions of all features cluster together in Pb-P-Cl space.

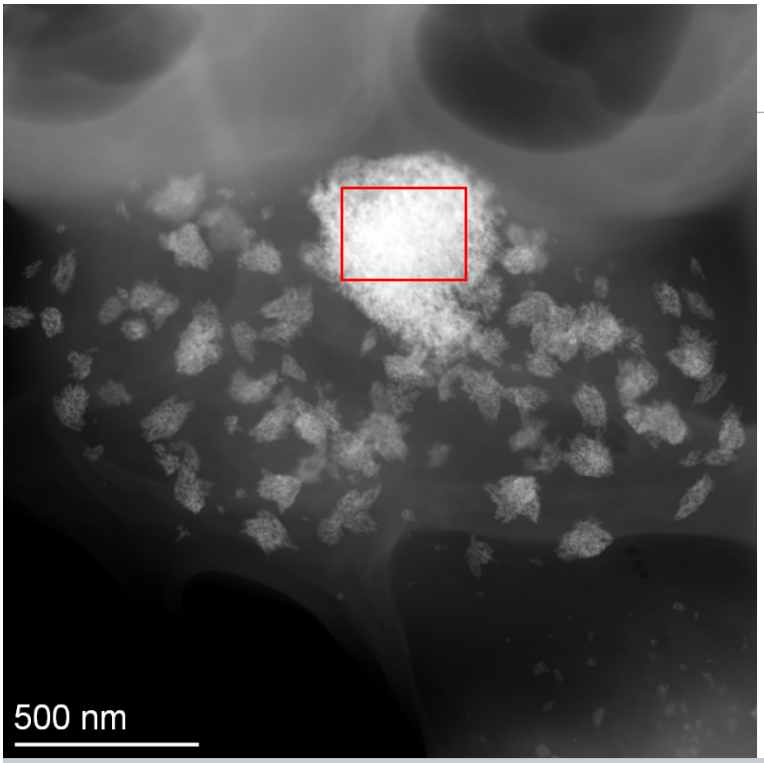

Element	Atomic Fraction (%)	Atomic Error (%)
C	40.53	11.16
N	5.13	1.38
O	24.26	5.82
Na	0.66	0.18
Mg	0.27	0.08
Al	0.56	0.15
Si	0.38	0.10
P	10.00	2.57
S	0.00	0.03
Cl	3.48	0.91
K	0.00	0.00
Ca	1.09	0.25
Fe	0.59	0.14
Pb	13.06	2.79

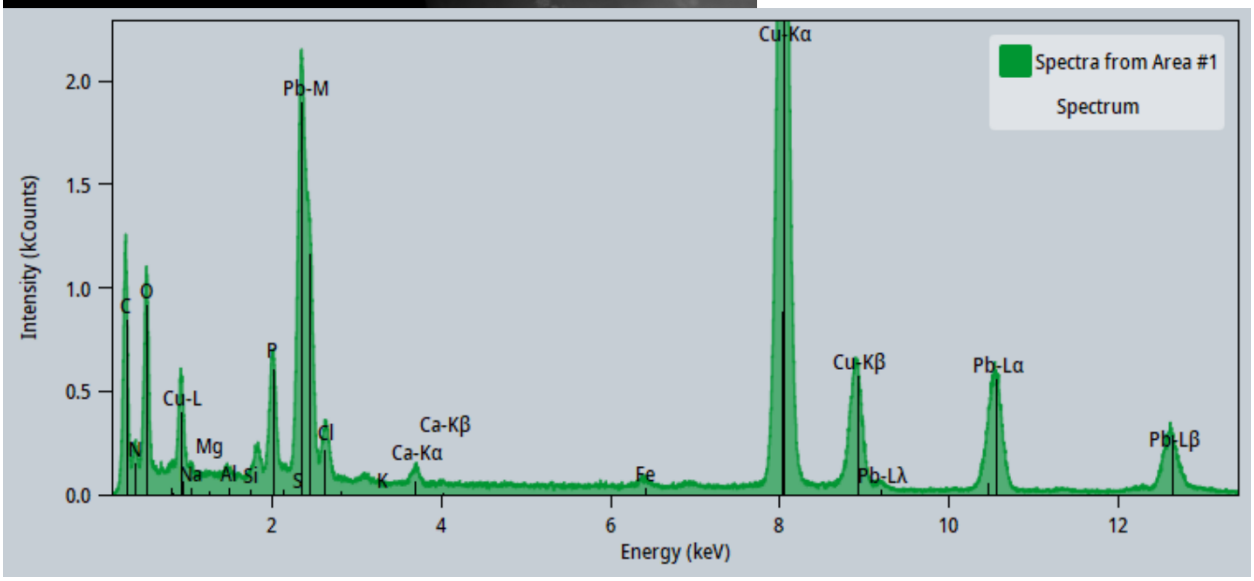

Figure 7. Tabulated atomic percentage values and EDS spectrum of a Pb-rich cellular feature. The analysis region was entirely within the largest bright feature in the upper middle of the image (red box). S quantification was not possible due to peak overlap with Pb M lines, and the large Cu peaks derive from the Cu TEM grids upon which cell samples were deposited. Note that C, N, and O have large atomic fractions because the specimen is biological in nature.

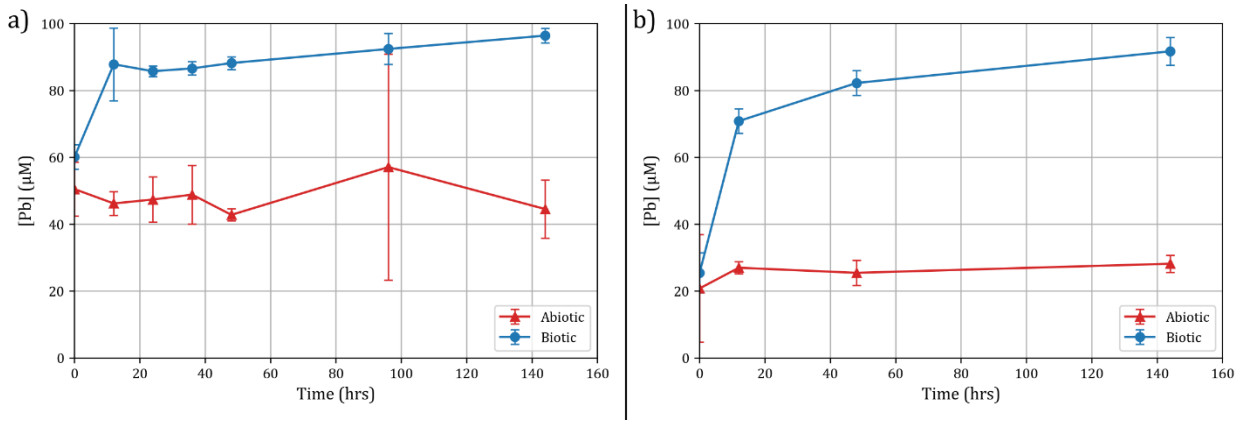

Figure 8a-b. Measured Pb concentrations in Pb-amended medium supernatants a) without filtration and b) filtration through 0.22 μm pore size PES membrane filters. The formulated Pb concentration was 100 μM. All error bars represent 95% confidence intervals from three replicate trials.

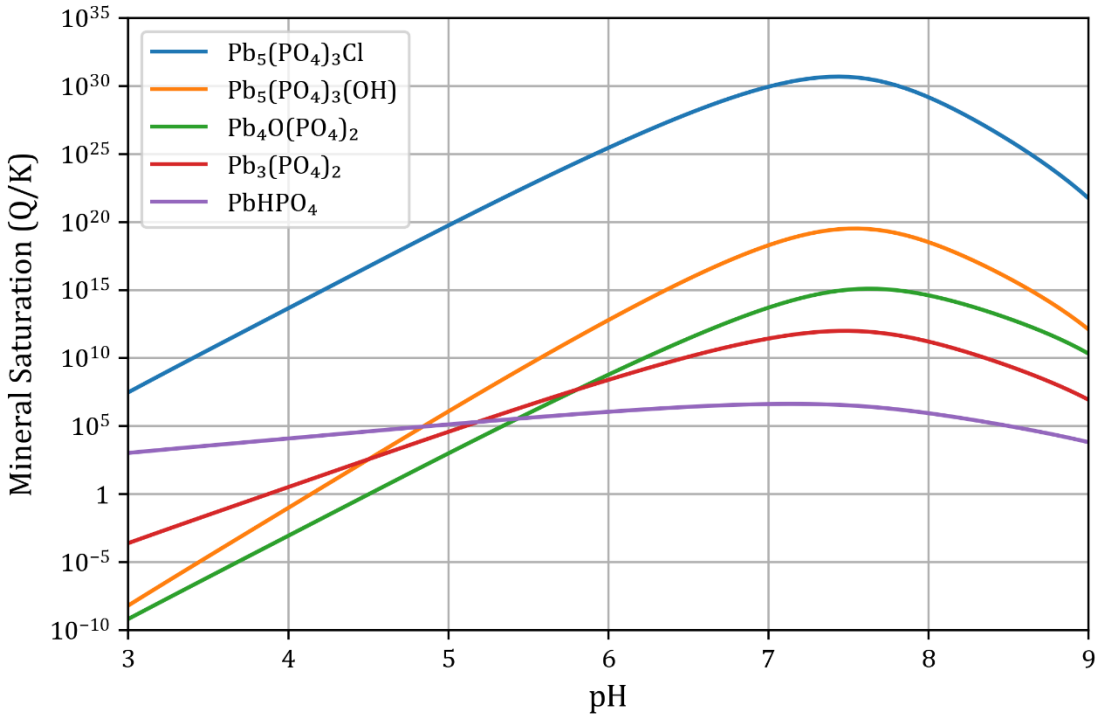

Figure 9. Saturation state of selected Pb-phosphate minerals in the P-containing (Pb-free) growth medium with additional 100 μM Pb modeled from pH 3 to 9 using GWB. Note that values greater than 1 represent mineral oversaturation while values less than 1 represent mineral undersaturation. While all selected minerals are supersaturated at the pH conditions of this experiment (5.6), pyromorphite [$Pb_5(PO_4)_3Cl$] has the highest saturation state and thus is the most thermodynamically favorable phase to precipitate from the modeled solution. The concentration of Na^+ was adjusted in the model to maintain charge balance as the pH was adjusted.

References

1. Agency for Toxic Substances and Disease Registry (ATSDR) (2020). Toxicological profile for lead. Atlanta, GA: U.S. Department of Health and Human Services, Public Health Service. https://doi.org/10.15620/cdc:95222.

2. Sparks, D.L. (2005). Toxic Metals in the Environment: The Role of Surfaces. Elements *1*, 193–197. https://doi.org/10.2113/gselements.1.4.193.

3. Jaishankar, M., Tseten, T., Anbalagan, N., Mathew, B.B., and Beeregowda, K.N. (2014). Toxicity, mechanism and health effects of some heavy metals. Interdisciplinary Toxicology *7*, 60–72. https://doi.org/10.2478/intox-2014-0009.

4. Egan, K.B., Cornwell, C.R., Courtney, J.G., and Ettinger, A.S. (2021). Blood Lead Levels in U.S. Children Ages 1–11 Years, 1976–2016. Environmental Health Perspectives *129*, 037003. https://doi.org/10.1289/EHP7932.

5. Ruckart, P.Z. (2021). Update of the Blood Lead Reference Value — United States, 2021. MMWR Morb Mortal Wkly Rep *70*. https://doi.org/10.15585/mmwr.mm7043a4.

6. Kundu, D., Mondal, S., Dutta, D., Haque, S., and Ghosh, A. (2016). Accumulation and contamination of lead in different trophic levels of food chain in sewage-fed East Kolkata Wetland, West Bengal, India. International Journal of Environmental and Technological Sciences *2*, 61–68.

7. Whittaker, E.J.W., and Muntus, R. (1970). Ionic radii for use in geochemistry. Geochimica et Cosmochimica Acta *34*, 945–956. https://doi.org/10.1016/0016-7037(70)90077-3.

8. Sicko-Goad, L., and Stoermer, E.F. (1979). A Morphometric Study of Lead and Copper Effects on Diatoma Tenue Var. Elongatum (bacillariophyta)1. Journal of Phycology *15*, 316–321. https://doi.org/10.1111/j.0022-3646.1979.00316.x.

9. Jensen, T.E., Baxter, M., Rachlin, J.W., and Jani, V. (1982). Uptake of heavy metals by Plectonema boryanum (cyanophyceae) into cellular components, especially polyphosphate bodies: An X-ray energy dispersive study. Environmental Pollution Series A, Ecological and Biological *27*, 119–127. https://doi.org/10.1016/0143-1471(82)90104-0.

10. Perdrial, N., Liewig, N., Delphin, J.-E., and Elsass, F. (2008). TEM evidence for intracellular accumulation of lead by bacteria in subsurface environments. Chemical Geology *253*, 196–204. https://doi.org/10.1016/j.chemgeo.2008.05.008.

11. Jroundi, F., Martinez-Ruiz, F., Merroun, M.L., and Gonzalez-Muñoz, M.T. (2020). Exploring bacterial community composition in Mediterranean deep-sea sediments and their role in heavy metal accumulation. Science of The Total Environment *712*, 135660. https://doi.org/10.1016/j.scitotenv.2019.135660.

12. Kulaev, I., Vagabov, V., and Kulakovskaya, T. (2008). The Biochemistry of Inorganic Polyphosphates, Second Edition. 211–268. https://doi.org/10.1002/0470858192.refs.

13. Kulakovskaya, T. (2018). Inorganic polyphosphates and heavy metal resistance in microorganisms. World Journal of Microbiology and Biotechnology *34*. https://doi.org/10.1007/s11274-018-2523-7.

14. Gupta, R.S., Patel, S., Saini, N., and Chen, S. (2020). Robust demarcation of 17 distinct Bacillus species clades, proposed as novel Bacillaceae genera, by phylogenomics and comparative genomic analyses: description of Robertmurraya kyonggiensis sp. nov. and proposal for an emended genus Bacillus limiting it only to the members of the Subtilis and Cereus clades of species. International Journal of Systematic and Evolutionary Microbiology *70*, 5753–5798. https://doi.org/10.1099/ijsem.0.004475.

15. Rathnayake, I.V.N., Megharaj, M., Krishnamurti, G.S.R., Bolan, N.S., and Naidu, R. (2013). Heavy metal toxicity to bacteria – Are the existing growth media accurate enough to determine heavy metal toxicity? Chemosphere *90*, 1195–1200. https://doi.org/10.1016/j.chemosphere.2012.09.036.

16. Biebl, H., and Pfennig, N. (1981). Isolation of Members of the Family Rhodospirillaceae. In The Prokaryotes: A Handbook on Habitats, Isolation, and Identification of Bacteria, M. P. Starr, H. Stolp, H. G. Trüper, A. Balows, and H. G. Schlegel, eds. (Springer), pp. 267–273. https://doi.org/10.1007/978-3-662-13187-9_14.

17. Hughes, M.N., and Poole, R.K. (1991). Metal speciation and microbial growth—the hard (and soft) facts. Microbiology *137*, 725–734.

18. Kumar Sani, R., Geesey, G., and Peyton, B.M. (2001). Assessment of lead toxicity to Desulfovibrio desulfuricans G20: influence of components of lactate C medium. Advances in Environmental Research *5*, 269–276. https://doi.org/10.1016/S1093-0191(00)00061-7.

19. Koch, A.L., and Crandall, M. (1968). Photometric Measurement of Bacterial Growth. The American Biology Teacher *30*, 481–485. https://doi.org/10.2307/4442152.

20. Widdel, F. (2010). Theory and Measurement of Bacterial Growth.

21. Allan, R.A., and Miller, J.J. (1980). Influence of S-adenosylmethionine on DAPI-induced fluorescence of polyphosphate in the yeast vacuole. Can. J. Microbiol. *26*, 912–920. https://doi.org/10.1139/m80-158.

22. Arighi, M., and Wilson, J.W. (1997). Comparative Effects of Fixation and Storage on Bone Tetracycline Fluorescence. Vet Comp Orthop Traumatol *10*, 200–204. https://doi.org/10.1055/s-0038-1632596.

23. Günther, S., Trutnau, M., Kleinsteuber, S., Hause, G., Bley, T., Röske, I., Harms, H., and Müller, S. (2009). Dynamics of Polyphosphate-Accumulating Bacteria in Wastewater Treatment Plant Microbial Communities Detected via DAPI (4′,6′-Diamidino-2-Phenylindole) and Tetracycline

Labeling. Applied and Environmental Microbiology *75*, 2111–2121. https://doi.org/10.1128/aem.01540-08.

24. Tiquia-Arashiro, S.M. (2018). Lead absorption mechanisms in bacteria as strategies for lead bioremediation. Applied Microbiology and Biotechnology *102*, 5437–5444. https://doi.org/10.1007/s00253-018-8969-6.

25. Jarosławiecka, A., and Piotrowska-Seget, Z. (2014). Lead resistance in micro-organisms. Microbiology *160*, 12–25. https://doi.org/10.1099/mic.0.070284-0.

26. Mitra, A., Chatterjee, S., Kataki, S., Rastogi, R.P., and Gupta, D.K. (2021). Bacterial tolerance strategies against lead toxicity and their relevance in bioremediation application. Environ Sci Pollut Res *28*, 14271–14284. https://doi.org/10.1007/s11356-021-12583-9.

27. Gadd, G.M. (2010). Metals, minerals and microbes: geomicrobiology and bioremediation. Microbiology *156*, 609–643. https://doi.org/10.1099/mic.0.037143-0.

28. Roane, T.M. (1999). Lead Resistance in Two Bacterial Isolates from Heavy Metal-Contaminated Soils. Microbial Ecology *37*, 218–224. https://doi.org/10.1007/s002489900145.

29. Levinson, H.S., Mahler, I., Blackwelder, P., and Hood, T. (1996). Lead resistance and sensitivity in Staphylococcus aureus. FEMS Microbiology Letters *145*, 421–425. https://doi.org/10.1016/S0378-1097(96)00443-0.

30. Keasling, J.D. (1997). Regulation of intracellular toxic metals and other cations by hydrolysis of polyphosphate. Ann N Y Acad Sci *829*, 242–249. https://doi.org/10.1111/j.1749-6632.1997.tb48579.x.

31. Aiking, H., Stijnman, A., van Garderen, C., van Heerikhuizen, H., and van 't Riet, J. (1984). Inorganic phosphate accumulation and cadmium detoxification in Klebsiella aerogenes NCTC 418 growing in continuous culture. Applied and Environmental Microbiology *47*, 374–377. https://doi.org/10.1128/aem.47.2.374-377.1984.

32. Sicko-Goad, L., and Lazinsky, D. (1986). Quantitative ultrastructural changes associated with lead-coupled luxury phosphate uptake and polyphosphate utilization. Arch. Environ. Contam. Toxicol. *15*, 617–627. https://doi.org/10.1007/BF01054908.

33. Zhang, Weixing., and Majidi, Vahid. (1994). Monitoring the cellular response of Stichococcus bacillaris to exposure of several different metals using in vivo 31P NMR and other spectroscopic techniques. Environ. Sci. Technol. *28*, 1577–1581. https://doi.org/10.1021/es00058a007.

34. Hynninen, A., Touzé, T., Pitkänen, L., Mengin-Lecreulx, D., and Virta, M. (2009). An efflux transporter PbrA and a phosphatase PbrB cooperate in a lead-resistance mechanism in bacteria. Molecular Microbiology *74*, 384–394. https://doi.org/10.1111/j.1365-2958.2009.06868.x.

35. Klaproth, M.H. (1784). Von dem Wassereisen, als einem mit Phosphorsäure verbundenen Eisenkalke. In Chemische Annalen für die Freunde der Naturlehre, Arzneygelahrtheit, Haushaltungskunst und Manufakturen (Fleckeisen), pp. 390–399.

36. Templeton, A.S., Trainor, T.P., Spormann, A.M., Newville, M., Sutton, S.R., Dohnalkova, A., Gorby, Y., and Brown, G.E. (2003). Sorption versus Biomineralization of Pb(II) within Burkholderia cepacia Biofilms. Environ. Sci. Technol. *37*, 300–307. https://doi.org/10.1021/es025972g.

37. Sharma, J., Shamim, K., and Dubey, S.K. (2018). Phosphatase mediated bioprecipitation of lead as pyromorphite by *Achromobacter xylosoxidans*. Journal of Environmental Management *217*, 754–761. https://doi.org/10.1016/j.jenvman.2018.04.027.

38. Teng, Z., Shao, W., Zhang, K., Huo, Y., and Li, M. (2019). Characterization of phosphate solubilizing bacteria isolated from heavy metal contaminated soils and their potential for lead immobilization. Journal of Environmental Management *231*, 189–197. https://doi.org/10.1016/j.jenvman.2018.10.012.

39. Van Veen, H.W., Abee, T., Kortstee, G.J.J., Konings, W.N., and Zehnder, A.J.B. (1994). Translocation of Metal phosphate via the Phosphate Inorganic Transport System of Escherichia coli. Biochemistry *33*, 1766–1770. https://doi.org/10.1021/bi00173a020.

40. Rosenberg, H. (1987). Phosphate Transport in Prokaryotes. In Ion Transport in Prokaryotes, B. P. Rosen and S. Silver, eds. (Academic Press), pp. 205–248. https://doi.org/10.1016/B978-0-12-596935-2.50009-8.

41. Rensing, C., Sun, Y., Mitra, B., and Rosen, B.P. (1998). Pb(II)-translocating P-type ATPases *. Journal of Biological Chemistry *273*, 32614–32617. https://doi.org/10.1074/jbc.273.49.32614.

42. Borremans, B., Hobman, J.L., Provoost, A., Brown, N.L., and van der Lelie, D. (2001). Cloning and Functional Analysis of thepbr Lead Resistance Determinant of Ralstonia metallidurans CH34. Journal of Bacteriology *183*, 5651–5658. https://doi.org/10.1128/jb.183.19.5651-5658.2001.

43. Chen, I.-M.A., Chu, K., Palaniappan, K., Pillay, M., Ratner, A., Huang, J., Huntemann, M., Varghese, N., White, J.R., Seshadri, R., et al. (2019). IMG/M v.5.0: an integrated data management and comparative analysis system for microbial genomes and microbiomes. Nucleic Acids Res *47*, D666–D677. https://doi.org/10.1093/nar/gky901.

44. Bethke, C.M. (2008). Geochemical and Biogeochemical Reaction Modeling Second Edition. (Cambridge University Press).

45. Harper, M. (2015). python-ternary: Ternary Plots in Python. Zenodo. https://doi.org/10.5281/zenodo.594435.